NRIAG Journal of Astronomy and Geophysics (2016) 5, 106–123

National Research Institute of Astronomy and Geophysics

NRIAG Journal of Astronomy and Geophysics

www.elsevier.com/locate/nrjag

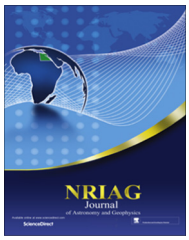

Application of high-pass filtering techniques on gravity and magnetic data of the eastern Qattara Depression area, Western Desert, Egypt

Hesham Shaker Zahra [a,*], **Hesham T. Oweis** [b]

[a] *Department of Geology, Faculty of Science, Banha University, Banha, Egypt*
[b] *Egyptian Natural Gas Company, Egypt*

Received 30 November 2015; revised 4 January 2016; accepted 27 January 2016
Available online 12 February 2016

KEYWORDS

Bouguer gravity;
RTP magnetic anomaly maps;
Polynomial surface fitting enhancement;
Laplacian;
Strike Filtering;
Enhancement Utilization;
Suppression Utilization;
Butterworth Filtering Utilization;
Butterworth high-pass filter techniques

Abstract In this work, a reconnaissance study is presented to delineate the subsurface tectonics and lithological inferences of the eastern area of Qattara Depression using the Bouguer gravity and aeromagnetic data. To achieve this goal, several transformation techniques and filtering processes are accomplished on these maps. At first, the total intensity aeromagnetic map is processed through the application of reduction to the magnetic north pole technique. The fast Fourier transform is carried out on the gravity and RTP magnetic data for establishing and defining the residual (shallow) sources. The frequency high-pass filtering is used to enhance the anomaly wavelengths associated with the shallow sources. The used processing techniques are the polynomial surface fitting enhancement, Laplacian, Strike Filtering, Enhancement Utilization, Suppression Utilization, Butterworth Filtering Utilization, Butterworth high-pass filter, Euler's deconvolution and forward modeling. The equivalent depths of the isolated short wavelength anomalies are 0.759 and 0.340 km below the flight surface, and the depths of the intermediate wavelength anomalies are 1.28 and 2.00 km for the gravity and magnetic data, respectively. Finally, the quantitative interpretations of the Bouguer gravity and RTP magnetic maps of the study area, reflect the occurrence of the various types of structures and their components. The main tectonic deformations of the study area have NNW–SSE, NNE–SSW, NE–SW, NW–SE and E–W trends.

1. Introduction

The investigated area lies in the northern part of the Western Desert of Egypt at a distance of about ten kilometers to the south of the Mediterranean Sea Coast, between latitudes 28°30′ and 30°00′N, and longitudes 27°30′ and 29°00′E (Fig. 1). The objective of gravity and magnetic interpretation was to recognize the geological characteristics of the

* Corresponding author.
Peer review under responsibility of National Research Institute of Astronomy and Geophysics.

http://dx.doi.org/10.1016/j.nrjag.2016.01.005

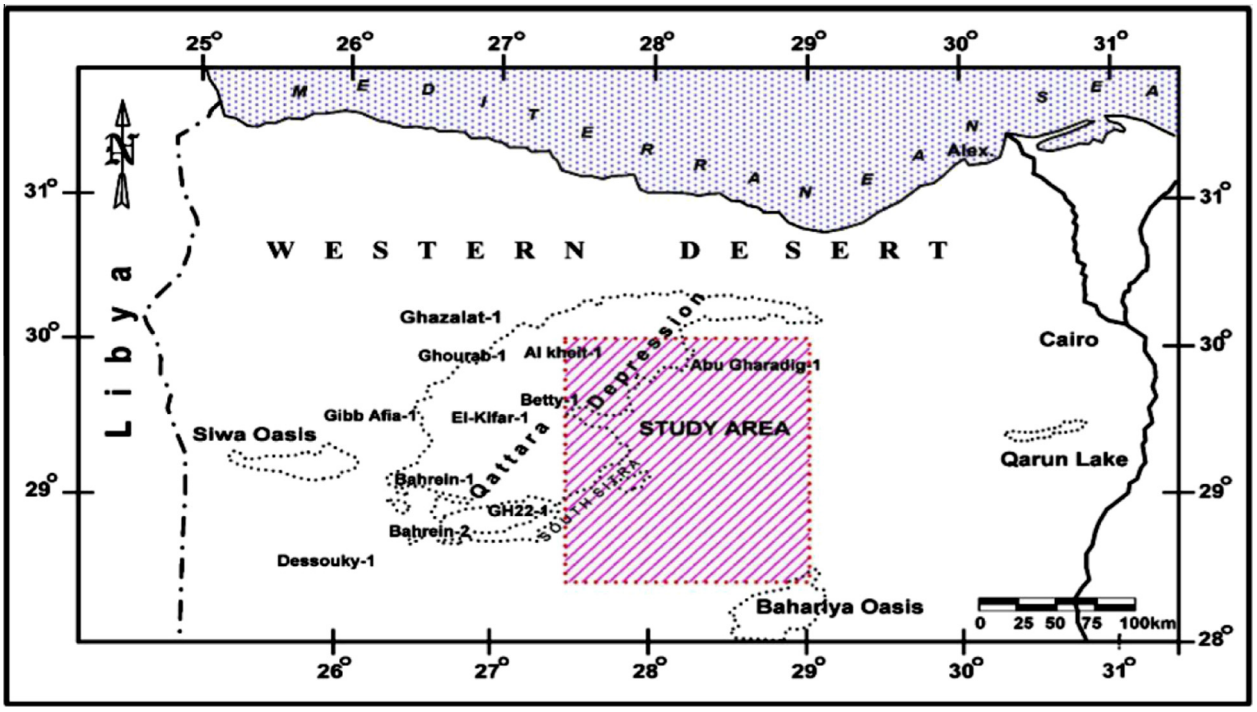

Figure 1 Location map of the study area.

subsurface lithologies and structures from the anomaly maps. This is to deduce, from the various characteristics (amplitude, shape, sharpness and frequency) of the gravity anomalies, the locations and structures that produce the gravity pattern. Gravity measurements have been used to follow many types of lithological and geological structures, ranging in depth and size from very deep crustal blocks to near-surface sedimentary elements. In addition, the magnetic prospecting is utilized to delineation of the intra-sedimentary and supra-basement magnetic sources, such as the shallow dykes and intrusives, that disrupt the normal continuity of the overlying sedimentary sequence.

2. Geological setting

Geomorphologically, the study area is a part of the northern Western Desert of Egypt and it may be regarded as a rocky platform of low altitude. In general, the Western Desert is essentially a plateau desert with vast expanses of rocky ground and numerous extensive and closed-in depressions (Said, 1990). The region exhibits a vast peneplain, which is covered in many places by wind-blown sand, sheets and gravels.

The main topographic features of the northern Western Desert are large plateaus slopping northwards closed-in depressions, oases and dunes (Abdine, 1974). The rocks and loose sediments cropping out on the investigated area belong to the Paleocene, Early Eocene, Middle Eocene, Late Eocene, Oligocene, Early Miocene, Middle Miocene, Late Miocene and Quaternary. All rocks are of sedimentary nature, although signs of volcanicity and hydrothermal activity are manifested, especially along fault lines. According to El Shazly et al. (1976), the outcrops of the study area are composed of rocks and loose sediments belonging to the Paleocene, Eocene, Oligocene, Miocene and Quaternary ages.

Stratigraphically, the Western Desert, with the exception of small outliner of Abu Roash, is a plateau covered with Neogene sediments (Hantar, 1990). Many recent activities of oil exploration works including drilling, seismic, gravity and magnetic measurements have reviled the presence of subsurface stratigraphic column, which ranges in age from Paleozoic to Recent. The generalized stratigraphic column of the northern Western Desert (Fig. 2) shows that the subsurface stratigraphic sequence is ranging in age from Cambro–Ordovician to Recent, resting unconformably over the crystalline basement rocks.

Tectonically, the northern Western Desert represents a part of the unstable belt of the tectonic framework of the Egyptian Territory. This area has been subjected to different tectonic regimes since the Paleozoic time, which resulted in the construction of many sub-basins, ridges, troughs and platforms.

3. Potential field data

The available gravity and magnetic data of the study area are as follows:

3.1. Gravity data

The Bouguer gravity anomaly map (G.P.C., 1985) with a scale of 1:100,000 and 1 mGal contour interval (Fig. 3), shows two strong positive anomalies shown at the central part, and a third steep positive gradient at the northern part of the map. The first one is exhibited as a closure trending ENE–WSW and extended to moderate positive anomaly toward the eastern border with E–W trend. The second positive anomaly extends to the north from the first one and shows more circular closure taking the WNW–ESE trend of 13 mGal amplitude. The last

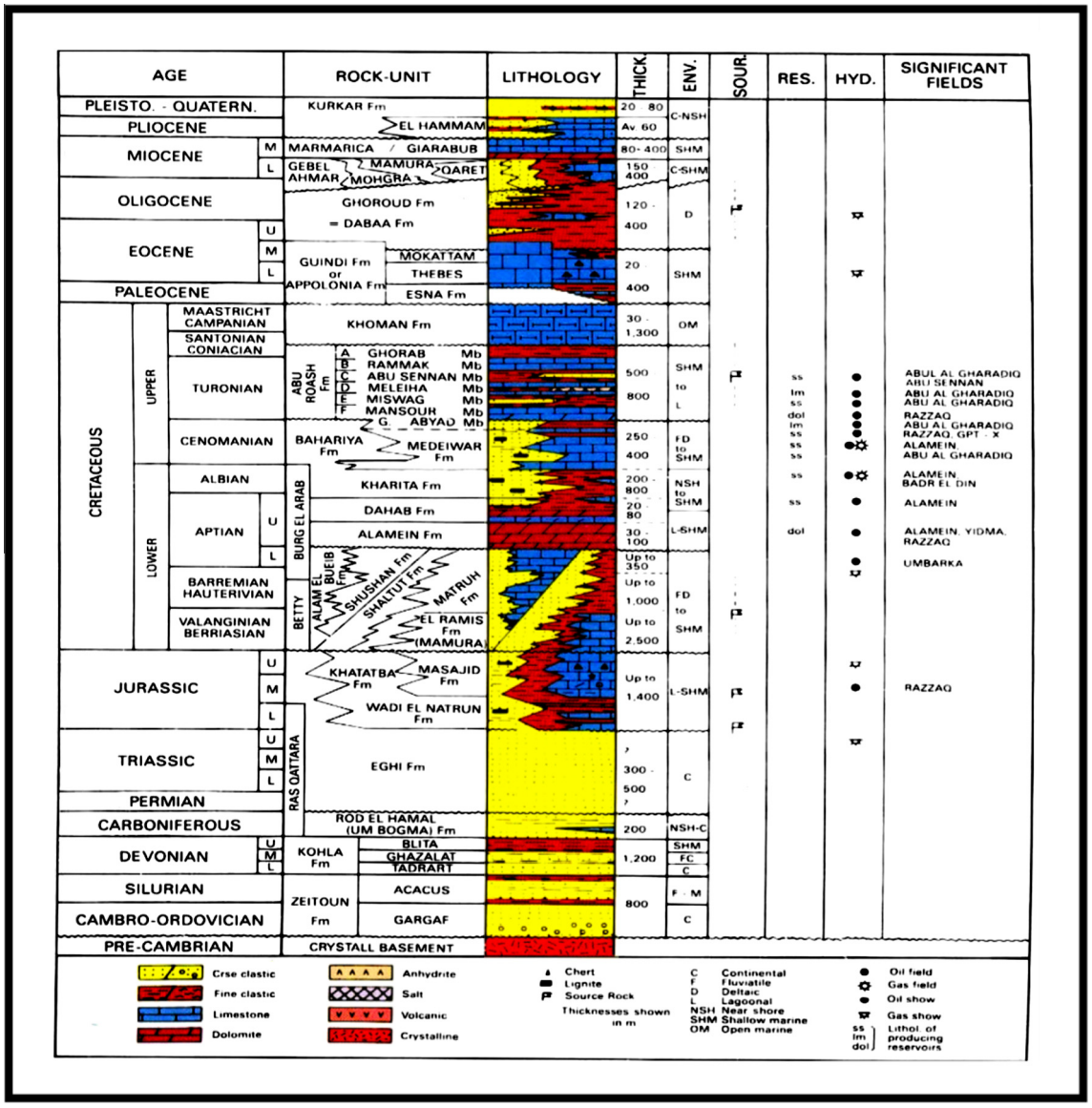

Figure 2 Subsurface stratigraphic column of the northern part of the Western Desert (Schlumberger, 1984).

positive gradient extends toward the northern and northwestern part of the map area in a semi-circular shape.

The Bouguer gravity anomaly map of the study area (Fig. 3) reflects that the gravitational field generally increases in center and northward direction. This may indicate that the crust-mantle boundary is deeper to the southwestern than the center and north or may be due to presence of more dense rocks to the northern of both.

3.2. Magnetic data

The total intensity magnetic map of scale 1:250,000, constructed using a contour interval of 5 nT is used in this study (Fig. 4). The present total intensity aeromagnetic map exhibits some different types of positive (red color) and negative (blue color) anomalies. The first is the strong positive and negative anomalies, which appears as contour closures.

Accordingly, the north part of the map area is occupied by the major positive magnetic belt, which is split into two larger positive closures as well as some small positive noises. The first anomaly trends nearly NE–SW with a maximum positive amplitude of 125 nT in the north western corner, while the second one is nearly irregular in shape at the northeastern part with maximum positive amplitude of 125–250 nT, which split into some circular noises. Moderate positive anomalies are included between the foregoing positive closures especially around Agnes anomaly.

However, the southern part of the map area reveals some major magnetic belts. The first major belt is a nearly NE–SW negative magnetic anomaly extending from the southeastern part of the map to south western part (blue color). This negative belt exhibits more than six local closures with negative amplitude ranged from −50 nT to −275 nT. Also, these anomalies demonstrate a condensing noising in its contour lines. Moreover, the southwestern corner of this belt is occu-

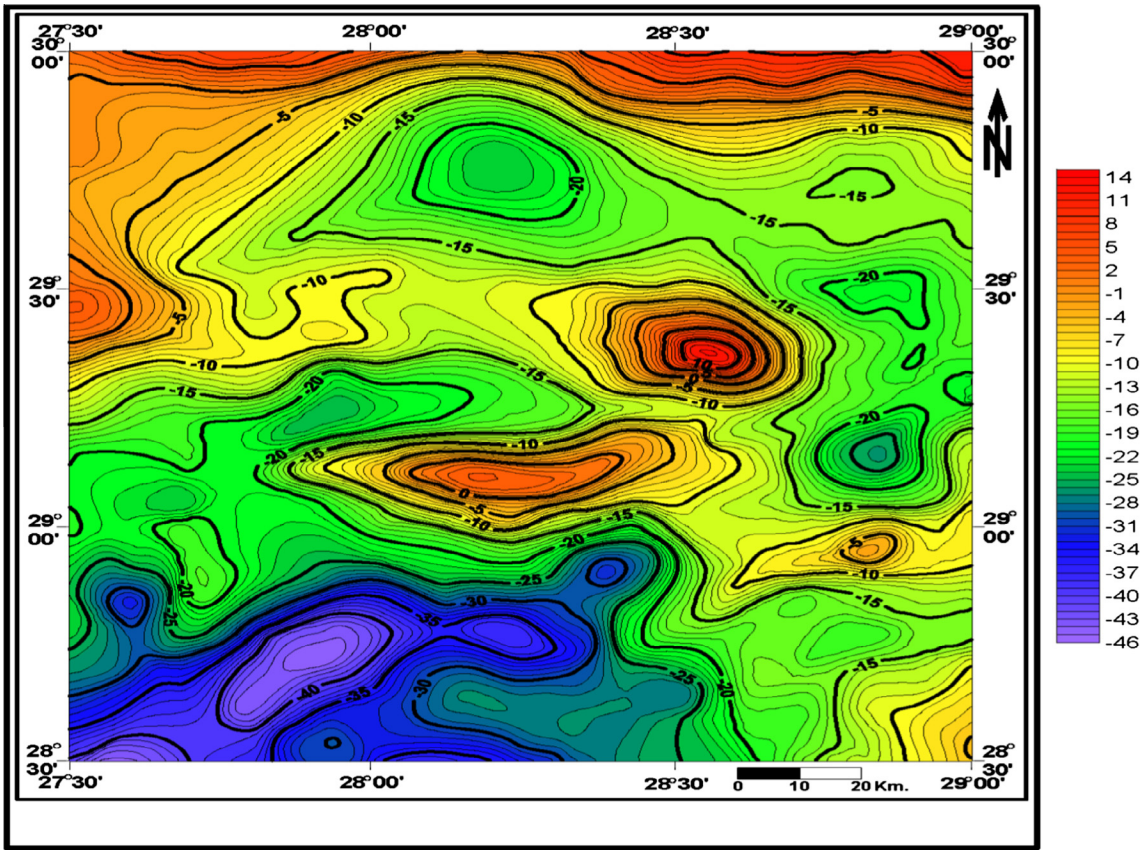

Figure 3 Bouguer gravity anomaly map of the study area.

pied by a low frequency elongated negative closure (blue color) with amplitude ranged from −75 nT to −150 nT.

Moreover, moderate NW–SE positive magnetic belt lies between the aforementioned two negative anomalies. Moderately steep magnetic gradient (green color) bounds the aforementioned southern negative magnetic belt and the northern positive magnetic belt.

4. Data processing of gravity and magnetic maps

4.1. Reduction to magnetic north pole

The shape of a magnetic anomaly, not only depends on the shape and susceptibility of the perturbing body, but also on the direction of its magnetization and their direction of the regional field. So, the RTP operation is used for centering the anomaly directly above the surface and the induced magnetization vector will be vertical downward exactly as gravity anomalies.

A reduction-to-the pole (RTP) transformation is typically applied to the total intensity magnetic data to minimize the polarity effects (Blakely and Simpson, 1995). Reduction-to-the pole is a filtering technique used to align the peaks and gradients of magnetic anomalies directly over their sources. In the present study, the total intensity aeromagnetic anomaly data are reduced to the magnetic pole (RTP), according to Geosoft Oasis Montaj 6.4.2 (2007) software.

A general outlook to the RTP map (Fig. 5), in comparison with the original total intensity aeromagnetic map (Fig. 4), reflects the northward shift in the positions of the inherited magnetic anomalies, due to the elimination of the inclination and their declination of the magnetic field at this area. Also, the sizes of the anomalies become larger and centered over their respective causative bodies to some extent. The magnetic gradients became more intensive and steeper, added to the increase of the anomalies reliefs, giving rise to more resolution in both the encountered lithologic and structural inferences. It worth mentioning that, the positive (red color) and negative (blue color) magnetic belts formerly described in the total intensity aeromagnetic map (Fig. 4) are well cleared and more perfectible in the RTP map (Fig. 5) with the appearance of some hidden anomalies.

4.2. Quantitative interpretation

The Bouguer gravity and RTP magnetic anomaly maps are subjected to several transformation and enhancement operations in the space domain comprising polynomial surface fitting enhancement, Laplacian, Strike Filtering, Enhancement Utilization, Suppression Utilization, Butterworth Filtering Utilization, and Butterworth high-pass filter techniques.

A pair of programs has been established for the filtering of the map data, in both space and frequency domains (Cooper, 1997), GravMap and PFproc programs. GravMap program takes data values from the scattered locations (such as gravity or magnetic stations), grids and contours to produce a map. This map may then be filtered using vertical continuation and polynomial surface fitting. In addition, linear profiles

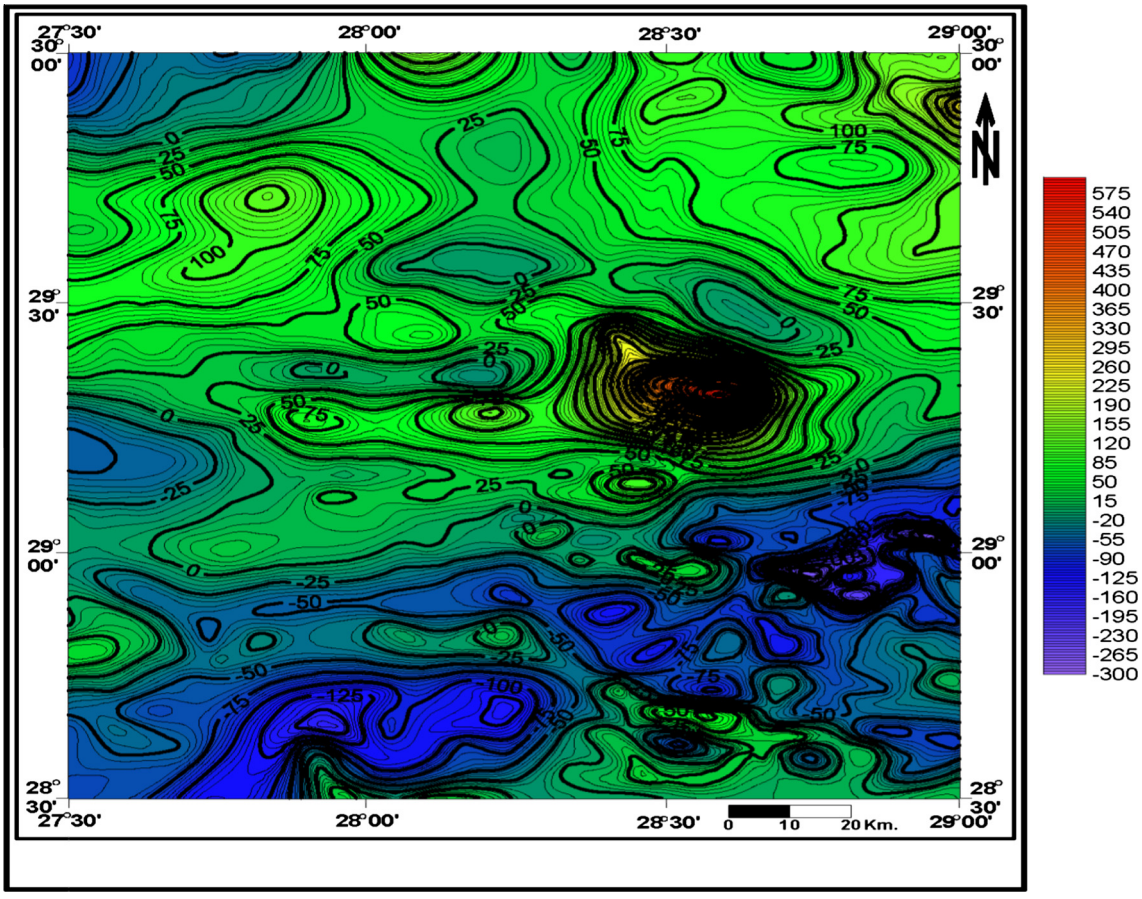

Figure 4 Total intensity aeromagnetic map of the study area.

may be generated at any angle across the map. PFproc program operates in similar manner to the GravMap program, in which the filters that may be applied to the data are strike filtering, vertical derivatives, sun-shading, low-pass and high-pass filtering and pole reduction.

4.3. Polynomial surface fitting enhancement

Trend surface is the geology profession name for a mathematical method of separating map data into two components, that of a regional nature and local fluctuations. The performances of orthogonal polynomial technique in the filtration of regional and residual anomalies have been evaluated with a view to minimizing personal biasing. The advantage of orthogonal over non-orthogonal polynomial is their ability to estimate an optimum order of polynomial to represent the predominant regional trend in the data using an approximate 2-D different table and the *z*-matrix (Agarwal and Sivaji, 1992).

The value of the trend surface can then be calculated at any point on the map and subtracted from the original data to give a residual map. Therefore, a fifth-order polynomial trend surface fitted to the Bouguer gravity and RTP magnetic data.

The fifth corresponding residual surface map remaining after each polynomial surface has been subtracted from the original gravity and RTP magnetic maps (Figs. 6 and 7). The residual map of the fifth-order polynomial trend surface of the gravity data (Fig. 6) represents a lot of spot-like local elements of high and low polarities, of smaller areal extensions, steeper surrounding reliefs, low or vertical amplitudes and the reduction in the anomalies sizes. These anomalies are, more or less, of higher frequencies, as the high positive anomalies in the central part of the map (red color). It is important to mention that, by using the polynomial method, the fifth order surface can be counted as the optimum for this operation. Therefore, these local anomalies may reflect comparable lithologic inferences and structural demonstrations in the sedimentary section and the related igneous bodies intruding this section.

The residual map of the fifth-order polynomial trend surface of the RTP data (Fig. 7) represents increasing the distribution of the spot-like local elements of high and low polarities, smaller areal extensions, reduction of the anomalies sizes and also increasing the small undulations (nosing) in the anomalies contour lines. Moreover, the map shows higher anomalies frequencies, sharper configurations and smaller magnitudes, as compared with the aforementioned residual maps. Generally, the surface at this order gives rise to the local elements more than the previous ones, as considerably in the southern and central parts of the map area (Fig. 7).

4.4. High-pass filtering operation

The gravity and RTP magnetic data are subjected to the second filtration process in the space domain, by using the high-pass filtering operators to enhance the signals

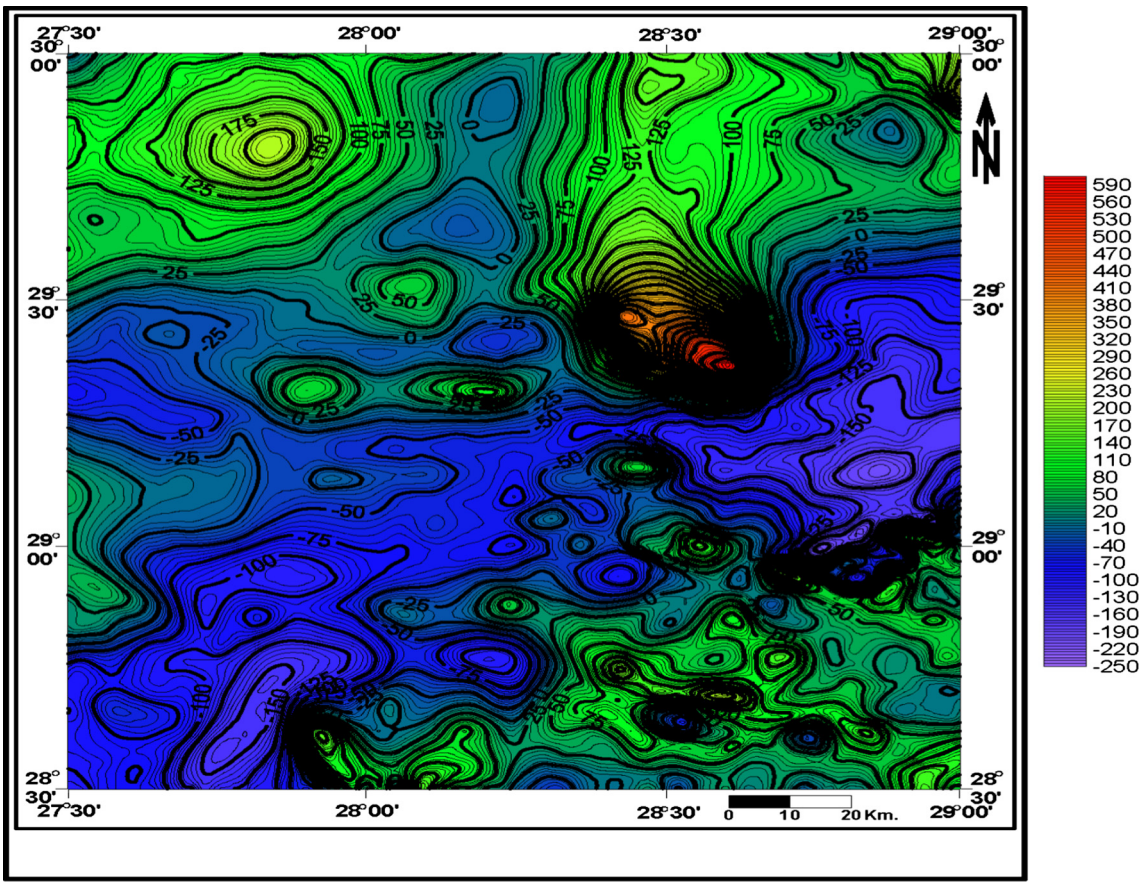

Figure 5 Total intensity aeromagnetic map reduced to the magnetic north pole.

characteristics of the available data. Filtration operation has a great important role in the different interpretation tools. The high-pass filters are used to bring out the details in the smoothed maps (as the risk of enhancing noise) using the Laplacian technique (Cooper 1997). This technique is applied on the data set grids by using the PFproc program.

4.5. Laplacian operator

The Laplacian operator produces a high-pass map for the given data, as given by Hord (1982). The Laplacian operator (Kernels) develops a high-pass gravity map (Fig. 8). This map shows that, the present area is distinguished by surficial or local anomalies (i.e. short wavelength anomalies) of shallow-seated sources, with sharp gradients and anomalies of relatively narrow irregular shapes. Mostly, these anomalies are presented in spot-like shapes of positive (red and yellow) and negative (light and dark blue) polarities and are often trending in the NE–SW, NW–SE, N–S and E–W directions for all the negative and positive anomalies. The produced high-pass filtered magnetic RTP map Fig. 9 reveals, more or less, the same shallow-seated anomalies (i.e. short wavelength and high frequency) in the spot like shapes, as correlated with the foregoing ones. These local anomalies are trending NE–SW, E–W, NW–SE and NNW–SSE, where the larger number of them is concentrated at the southeastern part, as well as some of them at the central part.

4.6. Strike filtering technique

Another type of filter is used to selectively suppress anomalies that are preferred azimuthally oriented. Features on a map that have a particular orientation may be enhanced by utilizing that strike filter. This is often useful to remove geological noises, such as dyke anomalies cutting across a feature of interest (Cooper 1997). Applied to anomaly data set, the directional filter tends to exaggerate and enhance trends in some chosen directions. Trends and alignments that are "discovered" in the data set by the use of such filter must, of course, be verified by referring back to the original data set (Dobrin, 1983).

As mentioned before, a directional filter such as strike filtering can be used to improve the features that have a particular orientation on a map. Such filter is helpful to inhibit the geological noises associated with certain geologic features, such as the dyke anomalies cutting across a sequence of interest. The angle 60° clockwise from the north has been used as the filter direction and severity levels (1, 2 and 3 km) are selected as filter elements for this application.

4.6.1. Enhancement Utilization

The resulted enhanced strike filtering features lying at angle 60° clockwise from the north and the aforementioned severity levels (1, 2 and 3 km). The gravity and RTP aeromagnetic data were countered and displayed in 2-D contour maps, and interpreted.

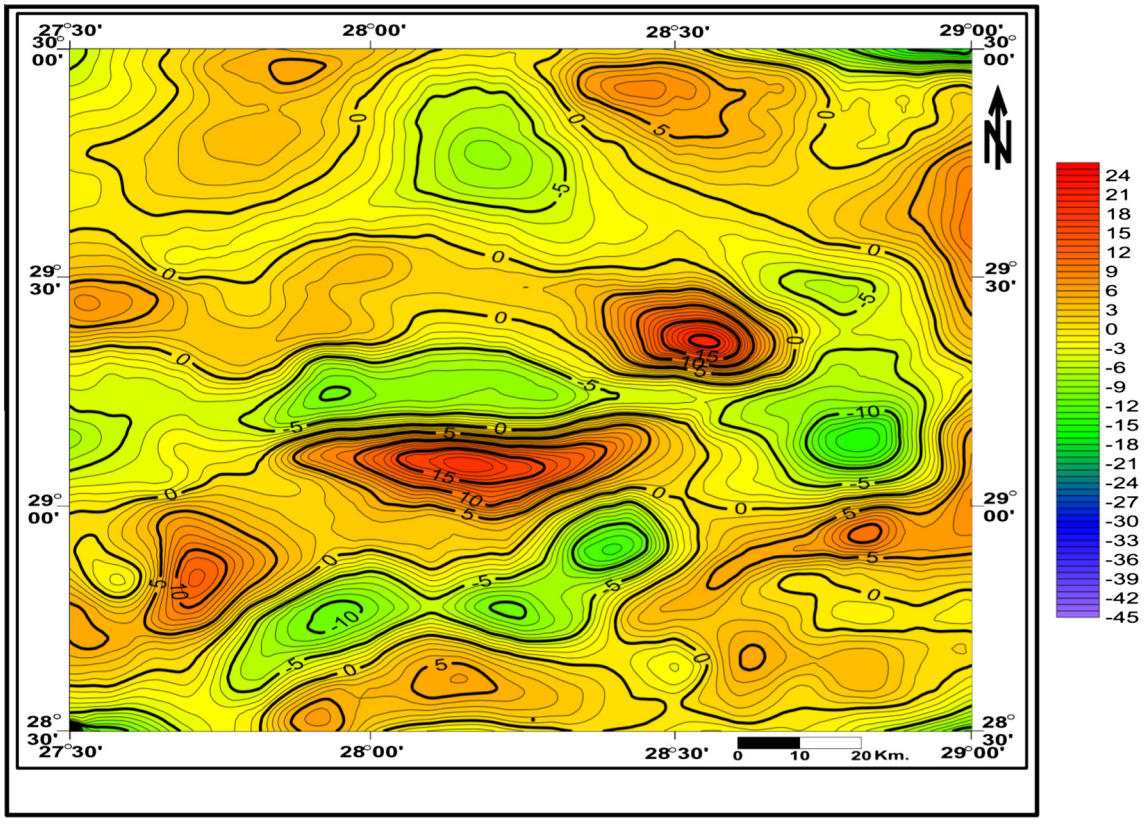

Figure 6 Residual map of the fifth-order polynomial trend surface fitted to the gravity data.

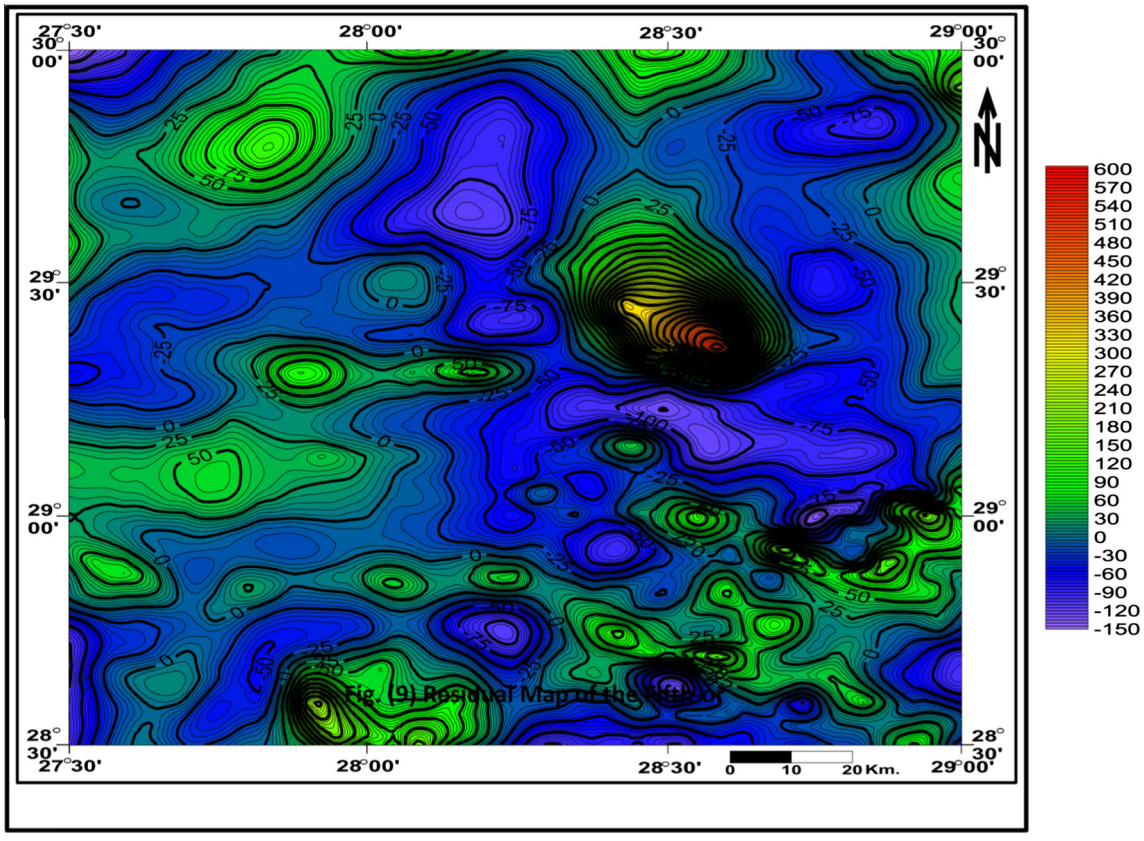

Figure 7 Residual map of the fifth-order polynomial trend surface fitted to RTP data.

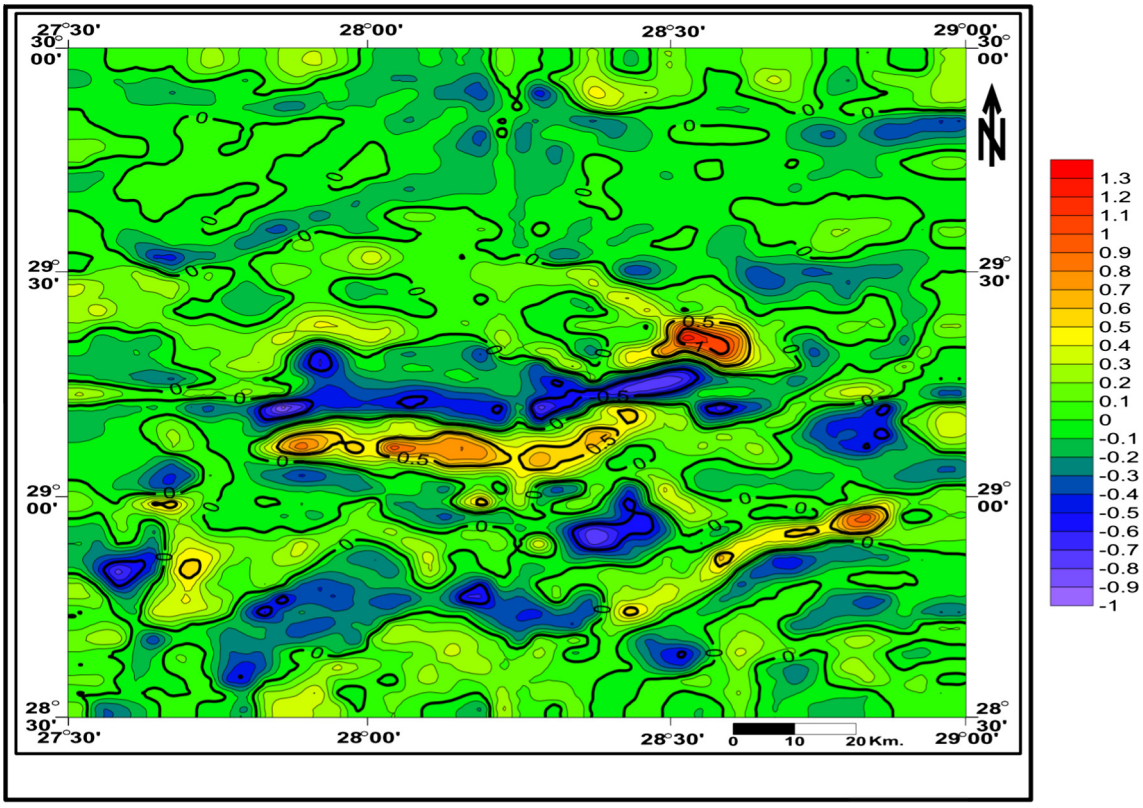

Figure 8 Laplacian high-pass filtered map of the gravity data.

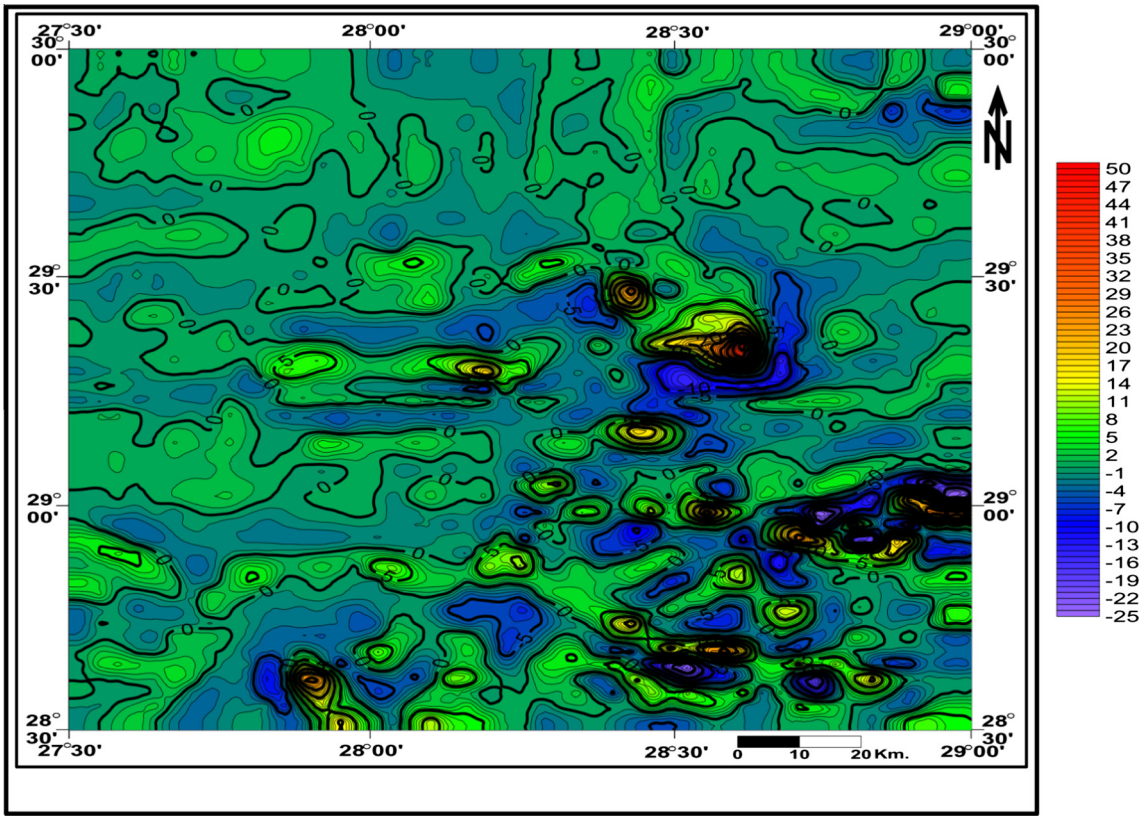

Figure 9 Laplacian high-pass filtered map of the RTP magnetic data.

1. The improved strike filtering features lying at angle 60° clockwise from the north and at 3 km in the gravity data (Fig. 10) reveal a better improvement for the long wavelength anomalies scattered in the map area and the complete attenuation of the short wavelength anomalies. Thus, the produced anomalies can be signified by smoothed contour lines, low reliefs and gentle gradients between them. It is important to point out that this map gives a good indication about the regional configuration of the study area.
2. The enhanced strike filtering features lying at angle 60° clockwise from the north and at 3 km in the RTP data (Fig. 11) reflect a better enhanced picture of the long-wavelength anomalies and attenuated the particularly oriented anomalies at this depth interval (3 km). So, the resulted anomalies are characterized by smooth and broad contour lines for their existence at larger depth. It is worth to mention that this map reveals a better regarding for the long-wavelength regional component.

4.6.2. Suppression Utilization

The property of the suppressed filter is similar to that of the enhancement filter, where this normally suppressed the redundant geologic noises from the significant ones.

In a comparable way of representation, the resulted suppressed strike filtering features lying at angle 60° clockwise from the north and at the three levels of severity (1, 2 and 3 km), and the gravity and RTP aeromagnetic data were contoured and displayed.

1- The suppressed strike filtering features lying at angle 60° clockwise from the north and at 3 km in the gravity data (Fig. 12) elucidate a valuable setting of the regional anomalies, as they become noise free, between or inside the major circular and elongated anomalies. Moreover, the map reflects a considerable attenuation in the reliefs and amplitudes of some of the dissipated anomalies.
2- The suppressed strike filtering features lying at angle 60° clockwise from the north and at 3 km in the RTP data (Fig. 13) reflect a better configuration of the regional components away from the effective particular noises and the small undulations in the inherited magnetic contours are mostly disappeared. Generally, the map reveals a reduction in the vertical reliefs, anomalies amplitudes and enlargement of the anomalies lateral extensions.

4.7. Butterworth Filtering Utilization

The Butterworth filter tool is applied in the frequency domain using different parameters through the Geosoft Oasis Montaj software version 6.4.2 (2007). The present Bouguer gravity and RTP aeromagnetic data are filtered using the Butterworth filter through the method parameters, degree of filter function is 8 (default), the central wave numbers of the filter are 0.03 and 0.042 (cycle/ground unit), respectively and 0/1 A flag (0 or 1), to specify whether a residual (0) high-pass is required, in which the maps will be discussed.

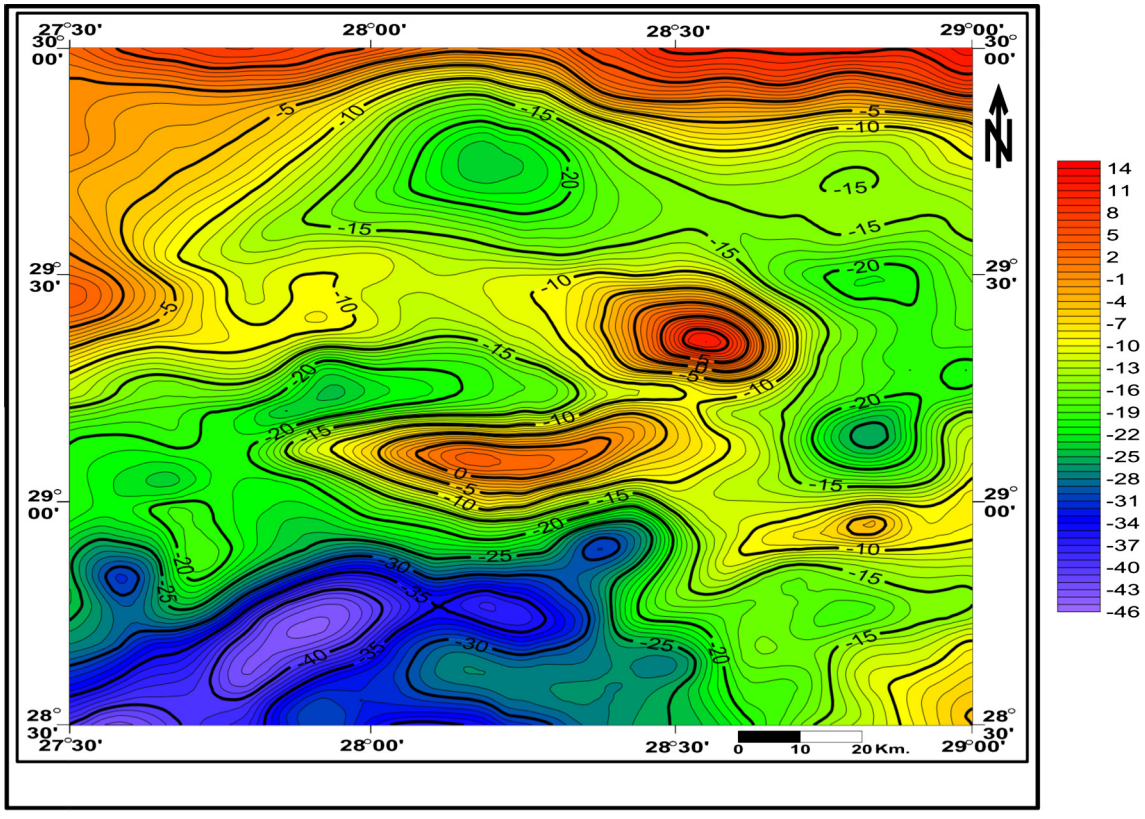

Figure 10 Enhanced strike filtering features lying at angle 60° clockwise north at 3 km in gravity data.

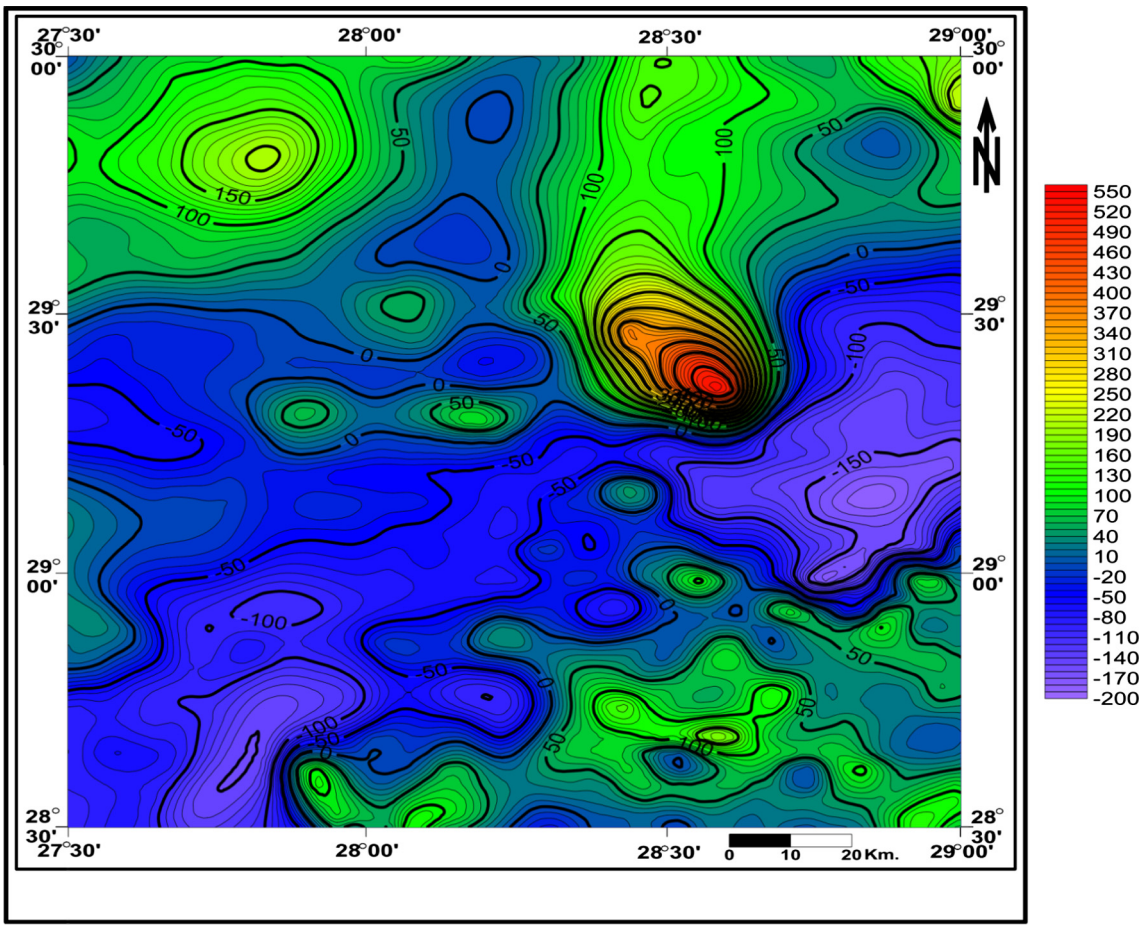

Figure 11 Enhanced strike filtering features lying at 60° clockwise from north at 3 km in RTP Data.

4.8. Butterworth high-pass filter

The high-pass gravity component map (Fig. 14) is characterized by several positive and negative gravity anomalies. These anomalies have semi-circular and elongated shapes and are located mainly at the central and southern parts of the area. This map shows linear gravity anomalies scattered all over the map and associated with shallow-seated tectonic structures. The trends bordering the residual anomalies are nearly E–W and occupied the central and northern parts, as well as NE–SW, N–S and NW–SE anomalies occupied the southern and western parts of the map area.

In the other direction, the high-pass magnetic component map (Fig. 15) clearly shows several spot-like positive and negative anomalies that have higher resolution than those of the RTP map. These anomalies have elongated, circular and nearly semicircular shapes and are signified by their relatively high frequencies and short wavelengths. The local variations in these anomalies characters may be due to the difference in their composition and/or their relative depths of their sources. These major trends, NE–SW, E–W, NW–SE and N–S directions, are recognized for the near-surface structures in the study area.

4.9. Euler's deconvolution

The advancement in acquisition techniques leads to routine collection of gravity and magnetic datasets (Hartman et al., 1971; and Reid et al., 1990). The large data volume demands automatic techniques like Werner (1953), Naudy (1971) and Euler deconvolution (Thompson, 1982) for the interpretation of gravity and magnetic anomalies. Euler deconvolution has emerged as a powerful technique for estimating the depth and geometry of the buried sources (Thompson, 1982; Reid et al., 1990). This technique has become popular, because it requires no a priori information about the source magnetization and it assumes no particular geological model. Thompson (1982) developed this technique for profile data, while Reid et al. (1990) extended it for gridded data.

The use of Euler deconvolution has emerged as a powerful tool for the direct determination of depth and probable source geometry in the gravity and magnetic data interpretations. The method can locate or outline the confined sources, dykes and contacts with remarkable accuracy. Euler deconvolution has been widely used in the automatic interpretation, because it requires no prior knowledge of the source direction and assumes no particular interpretation model.

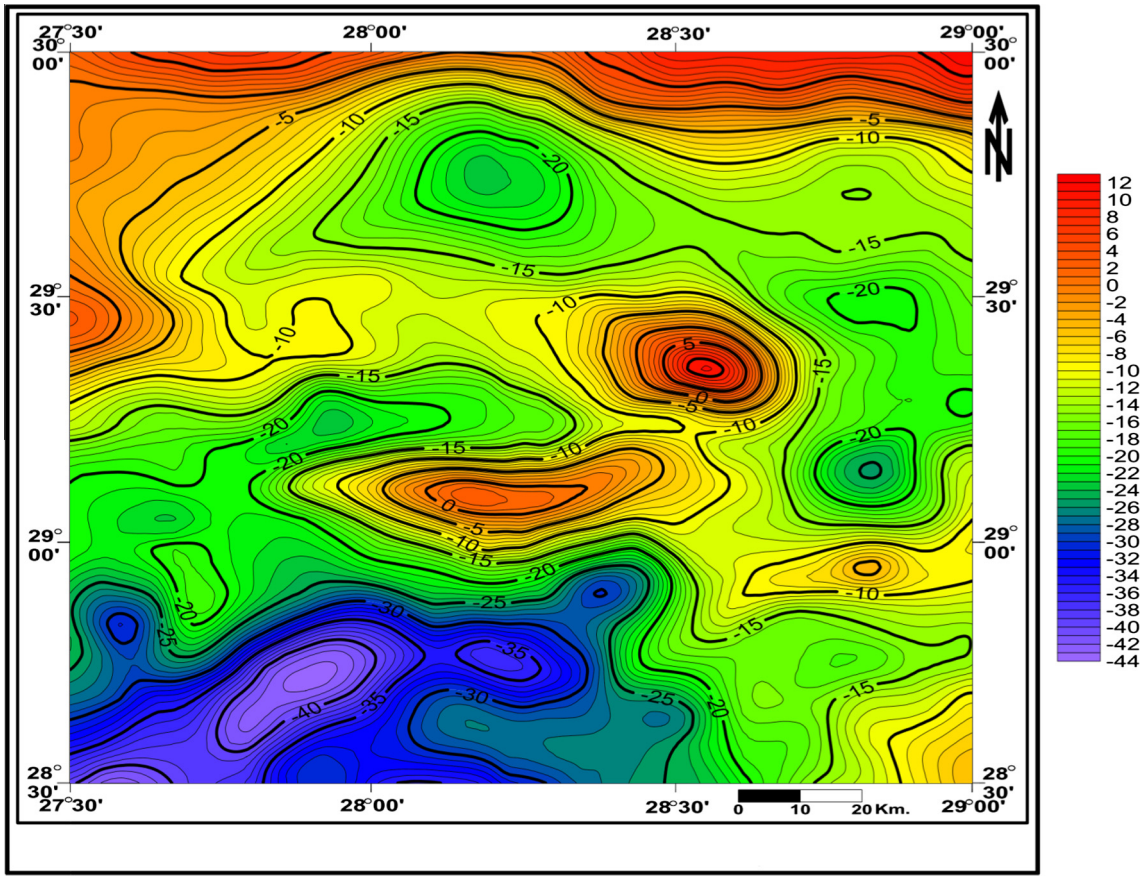

Figure 12 Suppressed strike filtering features lying at 60° clockwise from north at 3 km in gravity data.

The Euler deconvolution uses gradients to locate gravity edges and bodies, and estimate their depths, as well as the probable source geometry. The gravity map of the area is displayed as a color tone background in all these Euler maps to facilitate the comparison and interpretation. Investigation of these figures shows the general spatial correlation between the solutions obtained using the different structural indices.

Euler deconvolution method was applied to the gravity data using GRIDEPTH program, that included in the Geosoft Package (1994). However, the available Bouguer gravity anomaly map was subjected to this method using the structural indices (0.0, 0.5 and 1.0) and window size equal to 3, as well as tolerance value of 10.

However, the direct application of Euler deconvolution to magnetic data leads to unreliable and erratic results, because the magnetic field of an isolated body is seldom recorded in the field and is generally perturbed by the magnetic field of nearby bodies. Several authors (Thompson, 1982; Reid et al., 1990; Barbosa et al., 1999) have addressed this issue by assuming a constant regional background. This assumption introduces nonlinearity in the Euler equation. However, it can still be solved in a linear fashion by assuming tentative values of the structural index.

The structural index (SI) can be determined by observing the clustering of solutions for different SI values. For a particular feature, the correct SI yields a tight cluster. Reid et al. (1990) showed with the help of synthetic examples that, if an index is underestimated depth will also be underestimated and vice versa.

This method of estimating depths by varying the SI has become an accepted norm in geophysical literature (Barbosa et al., 1999). The use of tentative values of SI has prevented the technique from being fully automatic. The method has become subjective and time consuming as the interpreter has to judge the quality of clustering for different features as the index is varied.

An alternative approach is to estimate the source location, depth and SI simultaneously, assuming constant background (HSU, 2002; Gerovska et al., 2005). This approach is fully automatic and yields reliable estimates, if the background field can be adequately represented as a constant. However, the assumption of constant background is too simplistic, if the singular points are located close to each other.

The above problem was addressed by Stavrev (1997) by proposing an algorithm for linearizing the Euler equation with unprescribed structural index and linear background. The algorithm works on the principle of Differential Similarity Transform (DST). Gerovska and Araúzo-Bravo (2003) demonstrated the technique on a real and a synthetic dataset, modeled for a complex assemblage of simple magnetic bodies. They showed that simultaneous estimation of both the source coordinate and SI is possible using linear inversion, assuming linear background. In the synthetic example, however, some singular points show significant error in depth and SI due to the nonlinearity of the background field.

In this research, we propose to estimate both the source location and SI using the Euler deconvolution, assuming nonlinear background. We approximate the regional field

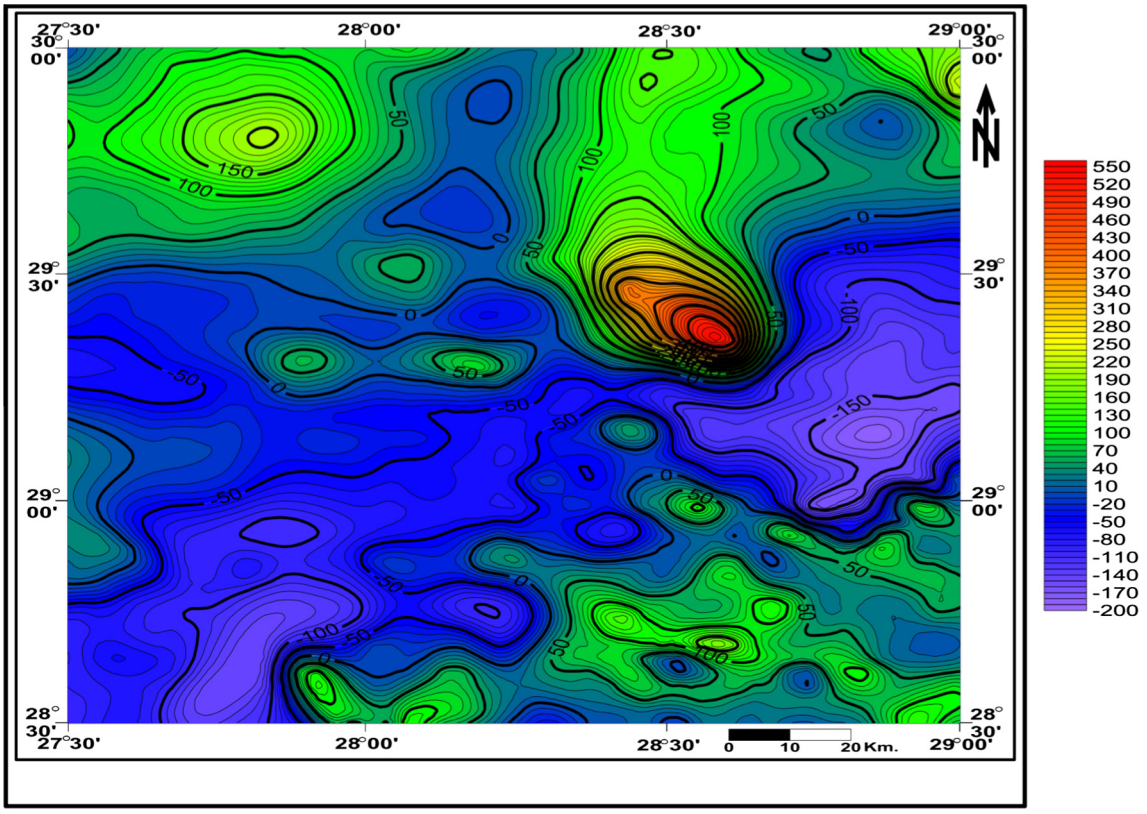

Figure 13 Suppressed strike filtering features lying at 60° clockwise from north at 3 km in RTP data.

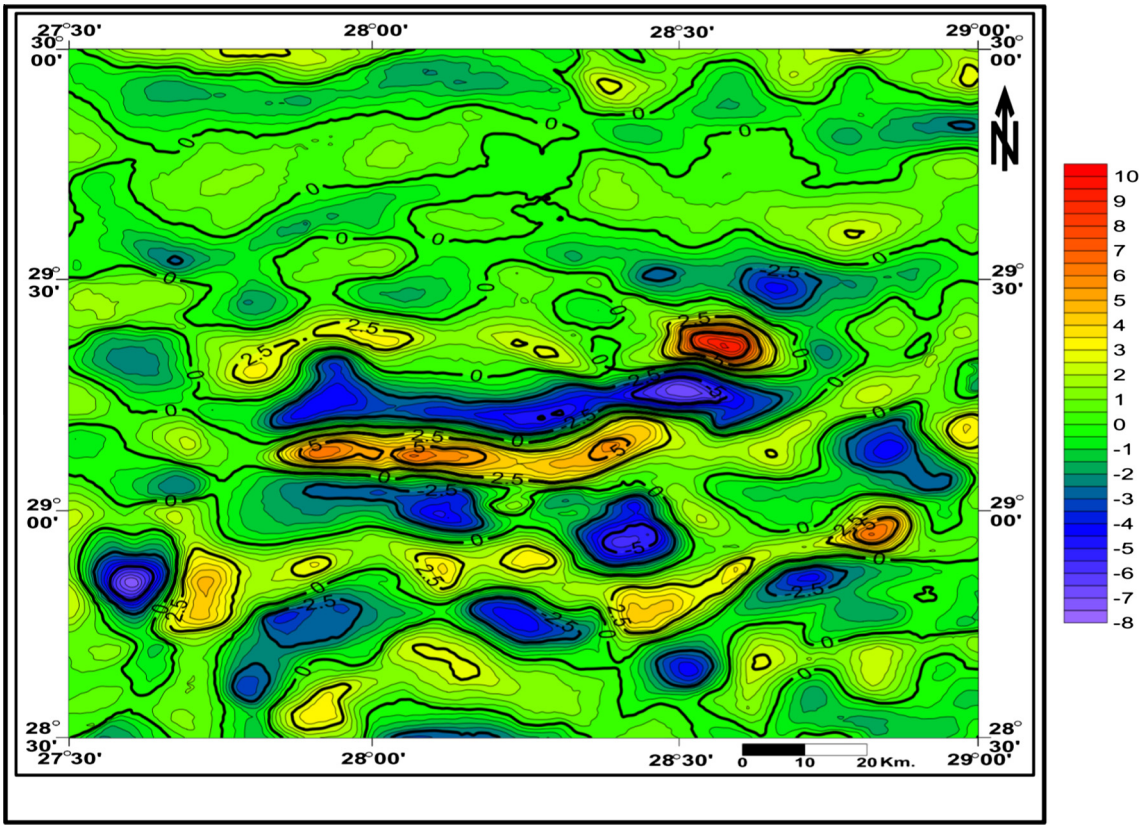

Figure 14 Butterworth high-pass filtered gravity map (Frequency cutoff = 0.03 cycle/km and 8.0 filter degree).

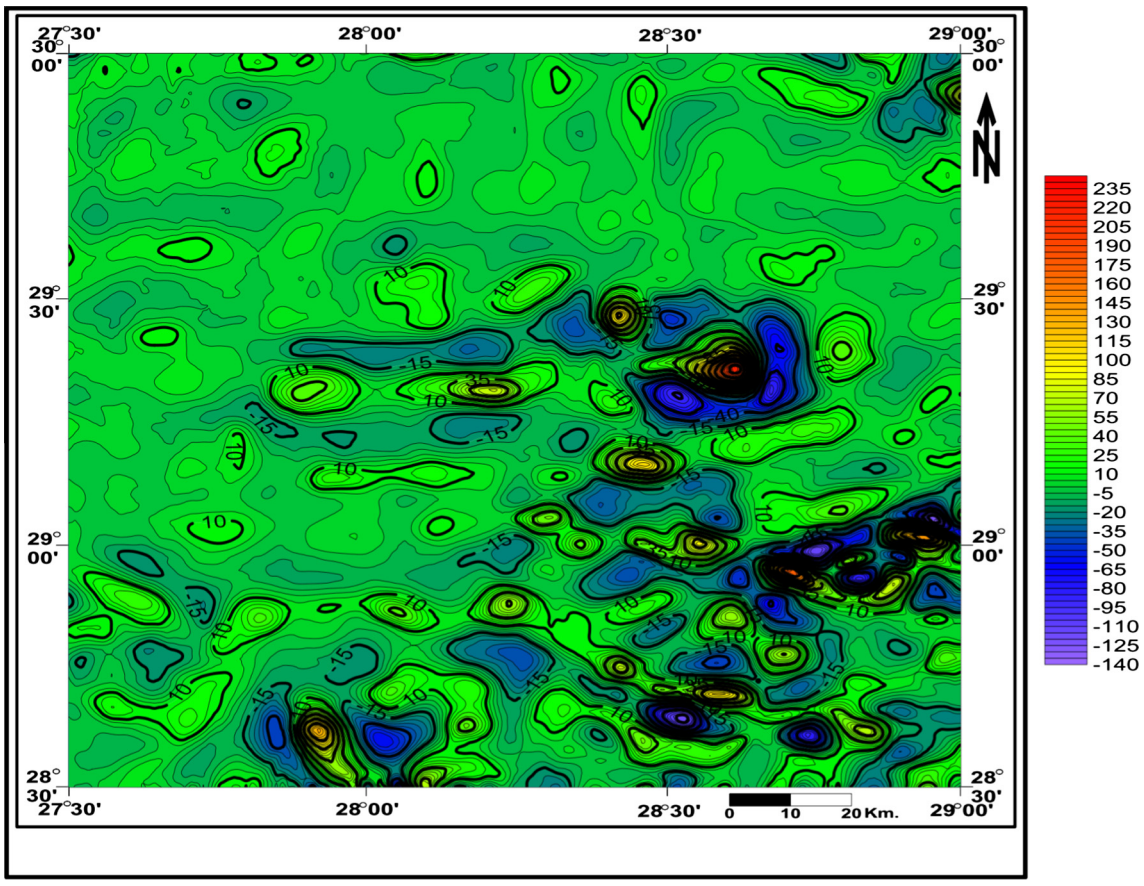

Figure 15 Butterworth high-pass filtered magnetic map (Frequency cutoff = 0.042 cycle/km and 8.0 degree).

using a rational function, in which both the numerator and denominator are linear. The Euler equation is solved in nonlinear fashion to estimate the source location, depth, SI and the coefficients of rational function. We apply the method to the same synthetic dataset, as used by Gerovska and Araúzo-Bravo (2003) and show, that the estimates of depth and SI for close by singular points have improved. The estimates of other singular points remain unaltered.

The most widely used norm to eliminate the spray of solutions is based on the standard deviation of the depth (Thompson, 1982), which can be estimated from the least-squares solution. Since, such an acceptance criterion is not possible for nonlinear inversion, we eliminated the erroneous solutions by using the criteria suggested by Silva and Barbosa (2003). They suggested that, the precision of depth and SI can be improved, if the computation is confined to the flat area of horizontal source location.

Fig. 16 gives a fine clue to the nature of the faulting features including their locations and depths. The structural index of SI = 0.5 is the correct value, generally yielding well focused solutions. The obtained solutions reveal a number of fault-like features at different depths within 1–5 km. The locations of clusters are distributed along the major geologic features in the map. These buried dykes are closely linked with the zones of dislocations and fracture systems between the major tectonic provinces. Moreover, new well clustered solutions are obvious in this map, trending in the NE–SW, NW–SE and N–S directions. The optimum depth solutions for these features range from 1 to 3 km (purple to light blue circles), which restricted at the southern and south central parts.

Fig. 17 displays the most possible locations and trends of the major faults affecting the basement rocks, with depths ranging from 1 to 5 km. The linear forms generally correspond to faults, whereas the contacts of circular forms limit the intrusive bodies.

These linear solutions possess the NW–SE, E–W and NNE–SSW directions as dominant trends all over the map area. This map shows a complex form of different circles, where the predominant depths are ranged from 1 to 3 km (blue and red colors) and concentrated at all parts of the map.

4.10. Forward modeling

The objective of interactive modeling technique is to create a geologic model on the computer screen (calculated) that is gravity and/or magnetic matching the observed anomaly profile. Each separate polygon assigns a certain density and/or susceptibility value. The anomaly along the entire profile is the sum of the contributions of each separate polygon.

The elucidation of gravity and magnetic anomalies is based on determining plausible shapes, positions and physical parameters for the geologic structures, which cause these fields. The problem of data inversion in its broadest sense requires conversion of the information, which has been obtained by measurements into geologic models. Essentially, an indirect modeling process is the calculation of the effect of the sample

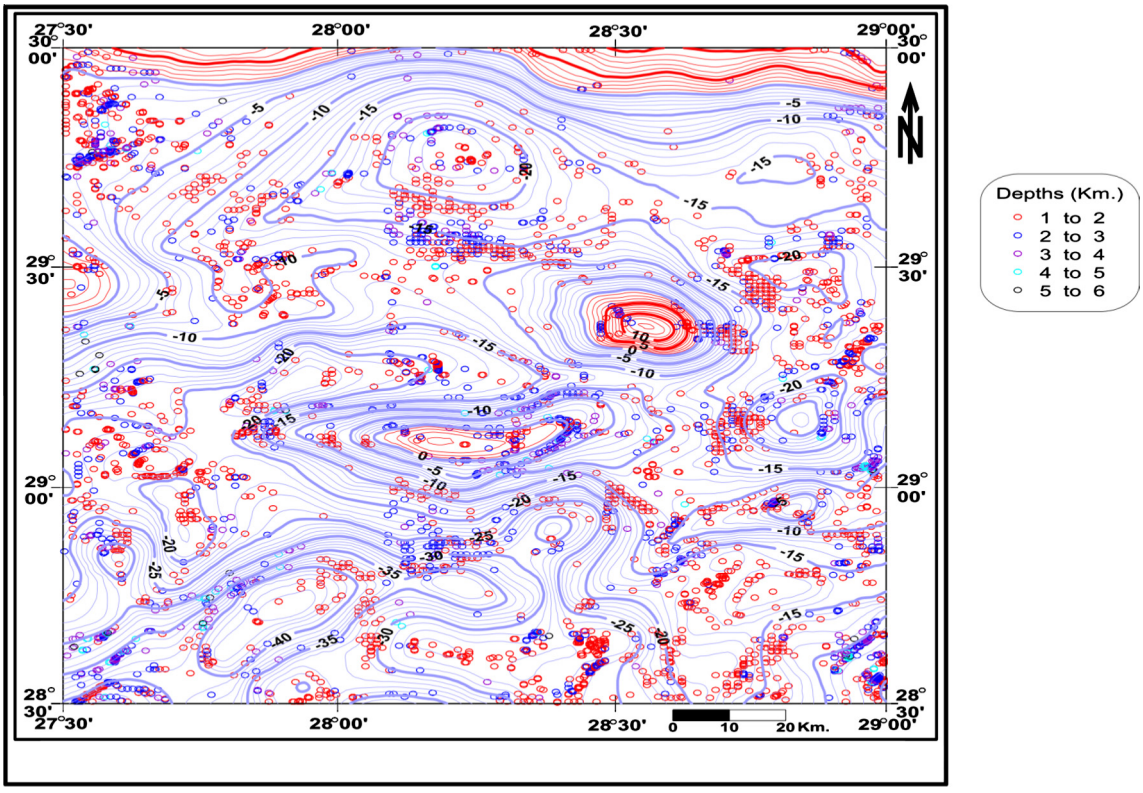

Figure 16 Step-fault locations and their depths deduced from Bouguer gravity using Euler deconvolution.

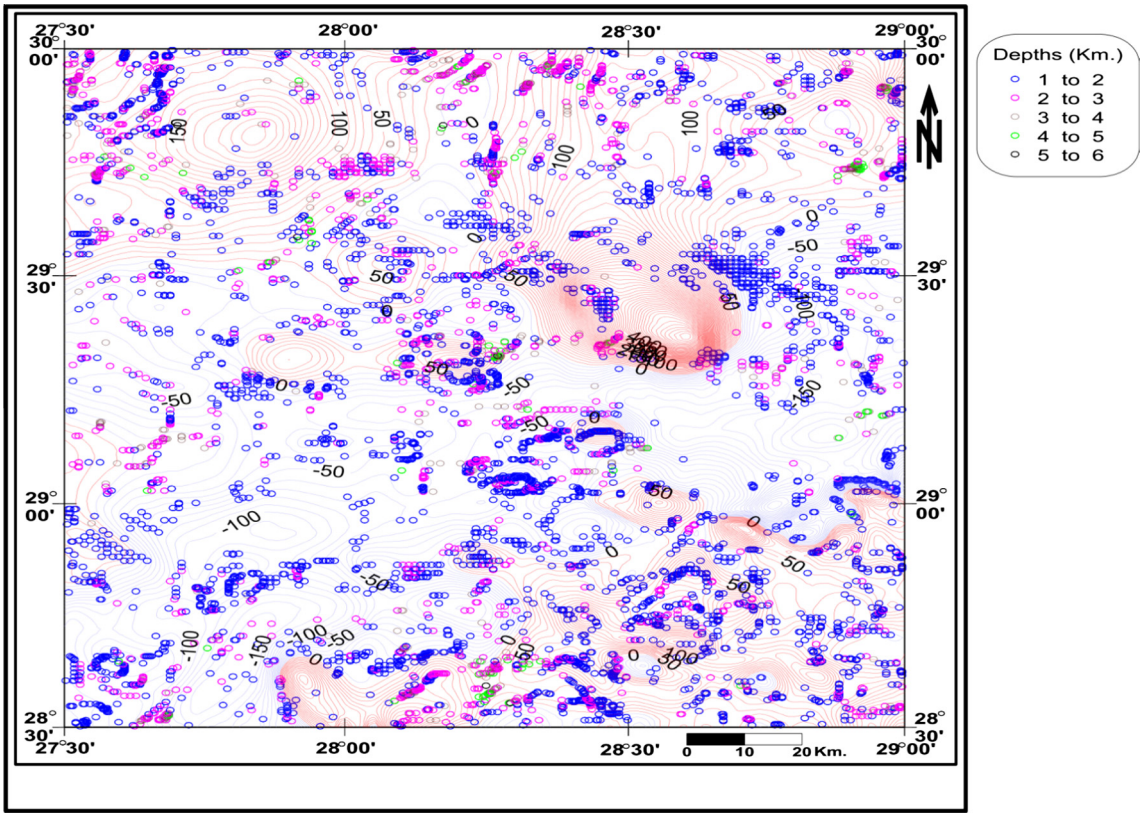

Figure 17 Step-fault locations and their depths deduced from magnetic map using Euler deconvolution.

elementary body, which approximates the geologic situation in the study area, followed by matching the model curve with the observed curve by trial and error graphic-interactive tools. The quantitative interpretation used a 2.5-D gravity/magnetic interactive modeling package running on GM-sys software (1994).

The Bouguer gravity values along five profiles were traced and used as the observed gravity profiles. Comparable profiles were taken in the same locations on the RTP magnetic map.

These profiles were taken along NW–SE, NE–SW and NNE–SSW directions, at right angles to the major geologic features. The potential fields (gravity/magnetic) were calculated iteratively for the basement structural cross-section until good fits were reached between the observed and the calculated profiles. Also, the modeling technique was achieved taking into consideration that, the bottom surface of the modeled polygons was assumed to be 6–7 km, in order to satisfy the regional effect in the investigated area.

The lithologic units of the basement complex in the study area can be viewed according to the classification of igneous rocks in terms of their susceptibilities. The lower susceptibilities (from 0.000153 to 0.000327 in cgs-units) and the densities (from 2.58 to 2.74 g/cc) are expected to be due to acidic rocks, while the high susceptibilities (until 0.0036 cgs-units) and the densities (until 2.84 g/cc) may be due to basic rocks. Here below is a brief discussion for the modeled profiles (BB′ and EE′).

4.11. Profile B–B′

The profile B–B′ (Fig. 18) runs through two major basinal areas, Abu Gharadig Basin to the east and Diyur Low to the west. It cuts laterally the NE–SW trend of the map area, as well as the major uplift of Sitra platform to the east central part of the study area.

The model shows a good tuning between the observed and calculated curves (either gravity or magnetic) along 175 km. The lower part of this model shows 21 proposed polygons varying in densities, susceptibilities and different depths.

The basement structure consists of several step-faulted blocks dipping toward the west and east, forming three grabens (basins) around two horsts (uplifts) structure

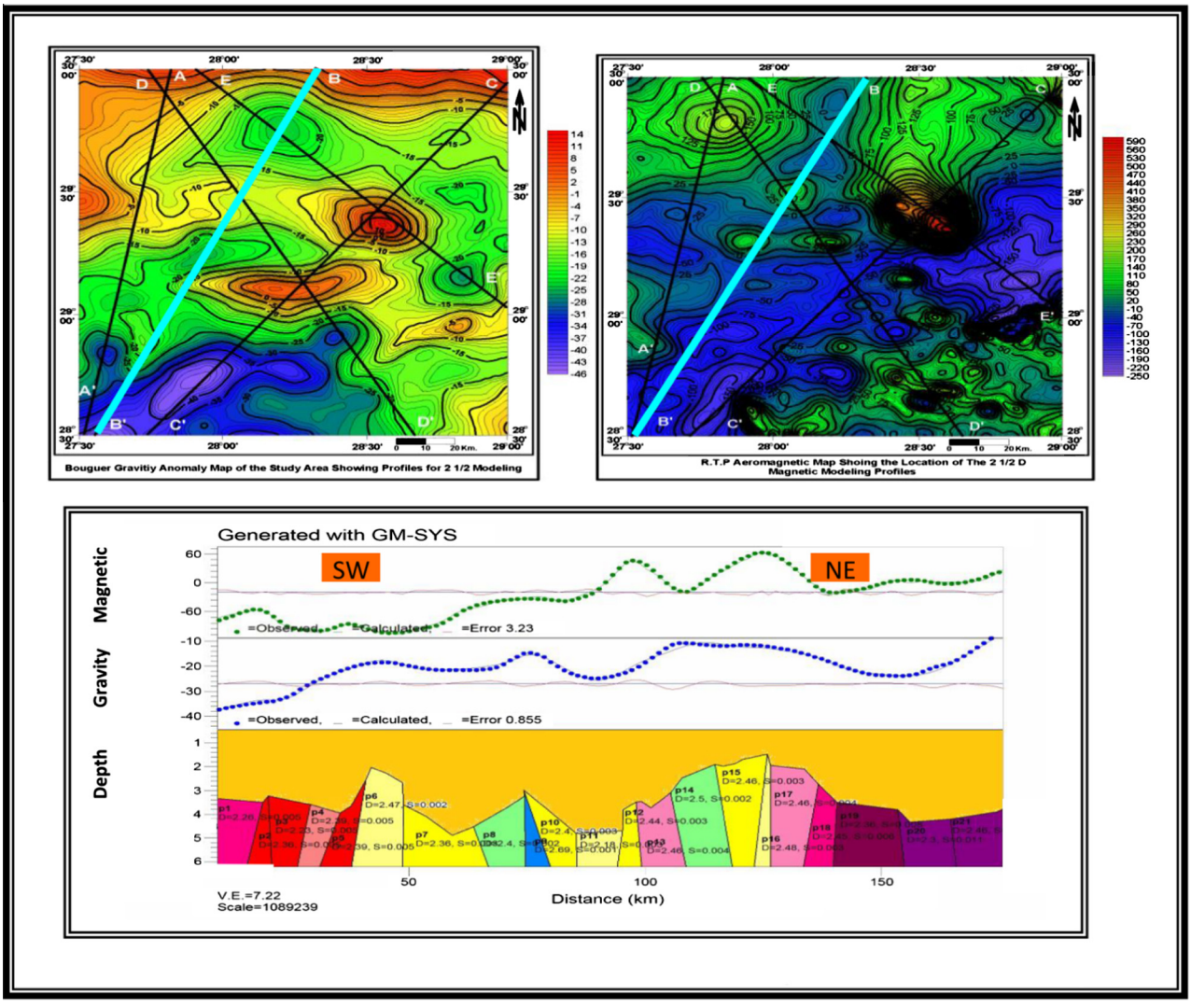

Figure 18 2½ Gravity and magnetic modeling along profile B–B′.

in-between. Generally, the magnetic maxima express the effect of anticlinal uplifts (horsts), whereas the basinal areas seem to be more corresponding to the gravity minima.

The basement blocks in the lower part show great variations in their rock properties. The magnetic susceptibility ranges from 0.001 cgs-units at P9 to 0.01 cgs-units at P20. The density contrast reaches the maximum beneath the east basinal area and the central uplifted one (P21 = 2.48 g/cc and P14 = 2.49 g/cc), while the lowest value is 2.18 g/cc at the center at P11. The sedimentary section reaches a thickness of about 4.8 km eastward (Abu Gharadig Basin and the central basins) and 3.4 km westward (Diyur low) before its thinning to about 1.5 km west of Abu Gharadig Basin. The model reveals that, the area is affected by intensive faulting of different throws and dips, and provides an evidence for the regional folding, that control the thickness of the sediments.

4.12. Profile E–E′

The profile is modeled in the NW–SE direction, which slices the study area into two parts, one at the northwest and the other at the southeast. Fig. 19 shows an excellent coincidence between both the observed and fitted curves, either gravity or magnetic. This fitness is conformable with the proposed structures in the lower portion. It was obtained by assuming 18 polygons, representing the uplifted and downfaulted basement blocks.

These tilted fault blocks differ from each other in its petrophysical parameters and configurations. They show lateral variation in the basement composition from acidic to basic (P12 = 0.001 and P15 = 0.014 cgs-units). The density values exhibit gradual increase toward the northern side (P3 = 2.26 g/cc and P9 = 2.6 g/cc). The maximum depth to basement (4.3 km) is recorded over the most down dip of the down-faulted graben (P2–P4) at the eastern end of Abu Gharadig Basin, as well as about 4.0 km at the south eastern part (Diyur low), while the minimum depth is about 1.0–1.6 km at the most up dip of the horst block (P11–P14), Agnes–Miswag ridge, and at Agnes horst. The profile indicates the presence of several faults of great throws and dips, in the form of horsts and grabens, has complicated the basement surface underlying the sedimentary section.

The high susceptibility and high density values of the basement rocks are sought to explain the strong positive gravity/magnetic amplitudes. The model indicates that, the

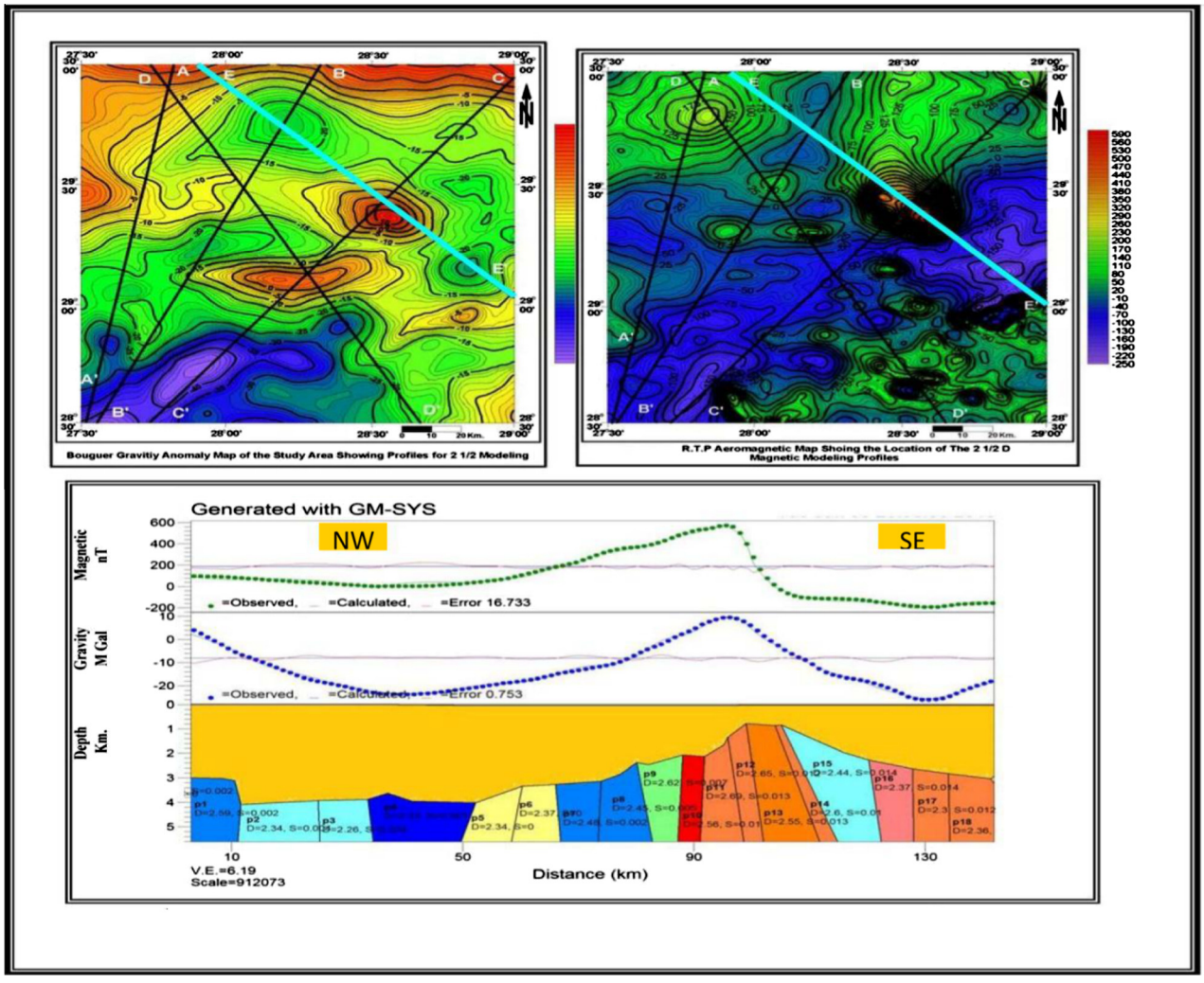

Figure 19 2½ Gravity and magnetic modeling along profile E–E′.

magnetic sources are dense and confirm that, the gravity source bodies are the sources of the magnetic anomalies.

In view of the foregoing discussions, the comparative study between the gravity and magnetic modelings indicates the following:

1. The study area can be divided into some major units of relatively simple and thick sedimentary cover beneath it, and more complicated basement structures made up of a number of swells and troughs. These segments are greatly differing in directions and dip regimes.
2. The models illustrate that, the basement rocks are mainly controlled by several normal faults at varying depths with different directions and throws. They indicate that, the most probable sites of thick sedimentation, in the form of structural basins, are linked with the lateral and/or vertical variations in the underlying basement rocks.
3. The modeled profiles provide evidence that, the basement fold structures play an essential role in the distribution of the sedimentary cover. Such structural setup of the basement affects the thickness variations in the sedimentary section, which in turn may have an effect on the hydrocarbon potentiality in the study area.
4. Several normal faults cutting the basement surface are traced, and the basement structures are interpreted as uplifts and basins and sub-basins. The most promising localities for petroleum potentialities and mineral exploration are those concerned with some high blocks of the major faults, which lying within or between the major tectonic provinces. The positive fault blocks inside the major basinal areas act as stratigraphic traps, where the chance of discovering giant oil fields is available.
5. These models suggest that, the basement rocks in the study area seem to be of acidic rock types intruded by some shallow and deep-seated basic intrusions. The basement complex lying in the northern part of the map shows a conspicuous basicity in the rock composition.
6. The results reveal that, the northern part of the study area shows regional thickening of the sedimentary section, with some exceptions. It is loaded by a thick sedimentary section, that may exceed 5.5 km in certain parts.
7. The models show that the basinal area in the northern part is almost associated with negative gravity anomalies as a result of the thick sedimentary cover and has positive magnetic characters since, it topped on basic basement rocks. They also reveal that, the anticlinal uplifts are associated with positive gravity and magnetic anomalies, because of the denser and more magnetized basement rocks have brought closer to the ground surface.

5. Conclusions

This paper deals with the evaluation of the lithological and tectonic setup of the eastern part of Qattara Depression, Western Desert, Egypt, from gravity and magnetic data. Several transformation techniques and filtering processes are accomplished on the Bouguer gravity anomaly and RTP magnetic map, through quantitative analyses. At first, the fast Fourier transform is carried out on the gravity for establishing Laplacian operation, the energy spectrum curve and defining the residual (shallow) sources. By the way, the frequency high-pass filtering is used to enhance the anomaly wavelengths associated with the shallow sources.

For optional separation of the signals, the high-pass filter is designed for each survey using the polynomial surface fitting enhancement, and strike filtering. The equivalent depths of the isolated short wavelength anomalies are 0.759 and 0.340 km below the flight surface.

The Euler deconvolution illustrates that the area is highly affected by these trends. Depths range from 1 km to more than 3 km below sea level. The 2.5D gravity modeling and analytical signal techniques confirm the depths to the gravity and magnetic sources deduced by the Euler method, whereas the depth to the basement rocks ranges from 0 km to about 3 km indicating that it is subjected to strong tectonic activities.

References

Abdine, A.S., 1974. Oil and gas discoveries in the Northern Western Desert of Egypt. In: 4th Exploration Seminar. E.G.P.C., Cairo, Egypt, pp. 1–27.

Agarwal, B.N.P., Sivaji, C.H., 1992. Separation of regional and residual anomalies by least-squares orthogonal polynomial and relaxation techniques: a performance evaluation. Geophys. Prospect. 40, 143–151.

Barbosa, V., Sliva, J., Medeiros, W., 1999. Stability analysis and improvement of structural index in Euler deconvolution. Geophysics 64 (1), 48–60.

Blakely, R.J., Simpson, R.W., 1995. Locating edges of source bodies from magnetic or gravity anomalies. Geophysics 51, 1494–1498.

Cooper, G.R.J., 1997. GravMap and Pf Proc software for filtering geophysical map data. Comput. Geosci. 23 (1), 91–101.

Dobrin, M.B., 1983. Introduction to Geophysical Prospecting. McGraw-Hili Book Co., New York, p. 630.

El Shazly, E.M., Abdel Hady, M.A., El Ghawaby, M.A., Khawasik, S. M., 1976. Regional Prospecting for Iron Ores in Baharia Oasis-El Faiyum area, Egypt, Using Landsat Satellite Images. Remote Sensing Center, Academy of Scientific Research and Technology, Cairo, Egypt, 16p.

General Petroleum Corporation, Egypt, 1985. Exploratory Report to the Compilation Gravity Isoanomaly Map of Egypt, Cairo.

Gerovska, D., Araúzo-Bravo, M.J., 2003. Automatic interpretation of magnetic data based on Euler deconvolution with unprescribed structural index. Comput. Geosci. 29, 949–960.

Gerovska, D., Stavrev, Y., Arauzo-Bravo, M.J., 2005. Finite-difference Euler deconvolution algorithm applied to the interpretation of magnetic data from northern Bulgaria. Pure Appl. Geophys. 162, 591–608.

Hantar, G., 1990. North western desert. In: Said, R. (Ed.), The Geology of Egypt. A.A. Balkema, Rotterdam, Brookfield, pp. 293–319 (Chapter 15).

Hartman, R.R., Teskey, D.J., Friedberg, J.L., 1971. A system for rapid digital aeromagnetic interpretation. Geophysics 36, 891–918.

Hord, R.M., 1982. Digital Image Processing of Remotely Sensed Data. Academic Press, New York, p. 256.

Hsu, S.K., 2002. Imaging magnetic sources using Euler's equation. Geophys. Prosp. 50, 15–25.

Naudy, H., 1971. Automatic determination of depth on aeromagnetic profiles. Geophysics 36, 717–722.

Reid, A.B., Allsop, J.M., Granser, H., Millett, A.J., Somerton, I.W., 1990. Magnetic interpretation in three dimensions using Euler deconvolution. Geophysics 55, 80–91.

Said, R., 1990. The Geology of Egypt. A.A. Balkema, Rotterdam, Brookfield.

Silva, J.B.C., Barbosa, V.C.F., 2003. 3D Euler deconvolution, theoretical basis for automatically selecting good solutions. Geophysics 68, 1962–1968.

Stavrev, P.Y., 1997. Euler deconvolution using differential similarity transformations of gravity or magnetic anomalies. Geophys. Prosp. 45, 207–246.

Thompson, D.T., 1982. EULDPH: a new method for making computer assisted depth estimates from magnetic data. Geophysics 47, 31–37.

Werner, S., 1953. Interpretation of aeromagnetic anomalies at sheet like bodies. Serv Geol. Undersok. Servo C., Arsbok 43 (6).